Spectrum estimation from truncated, non-linearly phase shifted or irregularly sampled interferograms

Alain Kattnig, Julien Jaeck, Olivier Gazzano, Jérôme Primot

Spectrum estimation from truncated, non-linearly phase shifted or irregularly sampled interferograms

ALAIN KATTNIG[1], JULIEN JAECK[1], OLIVIER GAZZANO[1], JÉRÔME PRIMOT[1]

[1]*DOTA, ONERA, Université Paris Saclay, F91123 Palaiseau - France*

Abstract: For performance or speed reasons, many types of spectrometers record only part of the interferogram thanks to its redundancy. Here we examine the consequences of this choice on the resulting spectrum. We jointly explore other sources of error also encountered on spectrometers, such as the irregular sampling of the interferometer and the non-linear phase of the spectrum. Then we revisit and improve the classical processing chain.

OCIS codes: (100.3175) Interferometric imaging; (110.4234) Multispectral and hyperspectral imaging; (150.1488) Calibration; (110.3080) Infrared imaging; (120.0280) Remote sensing and sensors; (300.6300) Spectroscopy, Fourier transforms

1. Introduction

Temporal Fourier Transform Spectrometers are tremendous tools for extracting spectral information from radiations [1]. However, the temporal exploration of the interferometric range by these spectrometers limits the accessible temporal resolution to a few seconds without giving up too high a spectral and radiometric resolution. In addition, the moving parts of such spectrometers are difficult to use in environments subject to strong vibrations, such as vehicles or aircraft.

One solution is to record only half of the interferogram thanks to their central symmetry. Going further means moving from spreading the variation of the optical path difference (OPD) over time to spreading it over the spatial dimension on an array of detectors [2,3,4]. But this solution drastically limits the possible spread of the OPD to the non-aberrant optical focal plane, thus limiting the spectral resolution. Once again we can record only part of the interferogram, increasing the spectral resolution. But this comes at a cost.

Here we present an analysis and a numerical model for spectrum reconstruction that explicitly takes into account the current errors that affect these systems, such as irregular sampling and phase errors. We rely on an existing instrument to work on realistic parameters, of the type we measured in the Sieleters instrument [5]. We will then evaluate the effectiveness of the correction steps. We will also study the spectral errors made by the usual Forman [6] and Mertz method [7]. We will then propose different, unfiltered solutions which will be evaluated.

Note that the spectrum estimators presented here were used in a previous paper in which we explored calibration issues in spatial calibration of static imaging Fourier Transform Spectrometers [8].

2. Asymmetrical and irregularly sampled OPD interferograms

Let us begin by detailing the reasons for these imperfect measures and then we will show how to simulate properly such measures.

2.1 Interferogram truncation and phase errors

Since the spectral resolution of Fourier transform spectrometers (FTS) is proportional to the maximum range of the optical path difference, it is worth increasing it by truncating the recorded interferogram. This is particularly the case for static FTS, as it is much more difficult to extend OPDs in space than in time. Extending OPDs in time means longer mirror displacement or a larger rotation range, depending on the apparatus [1]. But in order to extend the OPDs in spatial FTS we would need to widen the image plane to preserve the initial optical quality. This means more sophisticated and complex optics.

Such histogram truncation is possible due to the highly redundant nature of interferograms. Indeed, if we had "perfect" interferograms, only one side of the interferograms would be sufficient to compute the spectrum since in this case the interferograms are theoretically even (cf. Eq. (1)).

$$I(\delta) = \int_0^\infty L_\nu(\nu) \times \cos[2\pi\nu\delta] d\nu + \int_0^\infty L_\nu(\nu) d\nu \tag{1}$$

δ being the OPD, note that it can also be negative, being the difference between two optical paths. $L_\nu(\nu)$ being the spectral luminance of incoming radiation.

Unfortunately, there are many sources of error in this measure that break this symmetry. The best known are phase errors in the optics of the interferometer, electronics and sampling OPD errors [1], especially in spatial spectrometers where the OPD is not as easy to adjust as its temporal counterpart.

Fortunately, it is noted in the characterization of FTS instruments that the phase is slowly varying [1,6]. We believe that it is common to encounter this kind of situation because instrumentalists by seeking linearity spare us from this problem. Thus it becomes possible to estimate this phase from an interferogram with only a fraction of the range, thus making room for a much higher maximum OPD reached on a single interferogram wing (see Fig. 1).

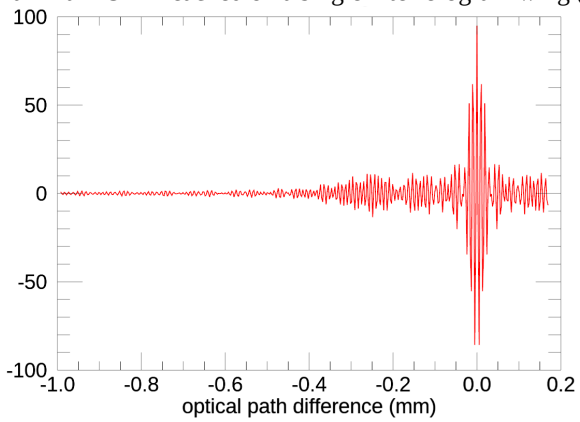

Fig. 1 : example of a truncated interferogram with the necessary symmetrical part to estimate the phase error.

Estimating and reconstructing the necessary data will inevitably have an impact on spectra SNR. Here we define the SNR as the ratio between the true spectrum and the difference between the true and the estimated spectrum.

2.2 Interferogram irregular sampling

Time FTS often have a very sophisticated laser-based OPD displacement measure [1], so irregular OPD sampling should not truly exist, unless by design (e.g. to increase spectral resolution and/or eliminate frequency folding).

But the spatial FTS is not so fortunate because sampling of the OPD by the focal plane array (FPA) will depend on actual position and orientation of the FPA as well as optical distortion. Thus spatial FTS using lenses in their optical design will be particularly exposed to irregular samplings [9].

3. Numerical based experiments

Experimental comparison of infrared spectra is a difficult subject because, even today, the optics of laboratory spectrometers are seldom cooled to cryogenic temperatures. Comparisons of high-precision spectra are therefore experimentally difficult to carry out. Fortunately, a large part of the potential errors can be studied mathematically and numerically through the use of models. This is the purpose of this paper.

To this end we have devised a synthetic spectrum with taxing properties, such as fast slopes (a in Fig. 2), an unresolved trough (region b), a large dynamic frequency chirp (region c) as well as non-linear phase error (cf. right part of Fig. 2).

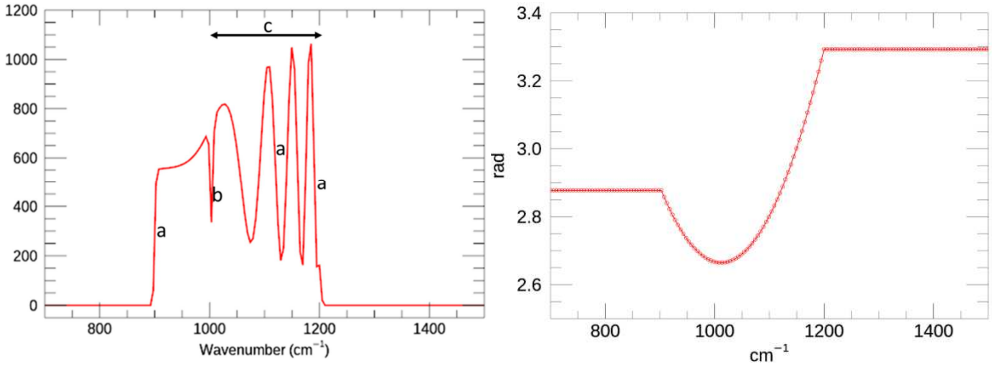

Fig. 2 : On the left is the synthetic spectrum used to test the entire spectrum interferogram signal processing pipeline. There are several fast ascending and descending slopes (a), an unresolved trough (b) and a large dynamic frequency chirp (c). On the right, we plot the slowly varying non-linear phase, with a dynamic range of 0.6 radians. Values outside the spectral range of [900-1250] cm^{-1} are undetermined and have been chosen constant for vizualisation reason. Due to the limited OPD range only 60 sampling points are available in the spectrum description on the instrument spectral range.

We have also chosen to stick as much as possible to real instrumental characteristics by mimicking the instrumental characteristics of the long-wave infrared Sieleters Fourier Transform Static Spectro imaging system [5]. In this case, the characteristics are mainly the spectral band, the phase of the spectrum and the OPD values on the Focal Plane Array. These last two parameters have been measured on the instrument [5] (see Fig. 5). Other than that the spectra amplitude has been chosen arbitrarily and has no unit.

Let's start by studying boundary effects which are particularly important in such an asymmetric signal.

3.1 Eliminating boundary effects

Processes making use of nearby samples, such as interpolation or Fourier transform, will be subject to signal boundary effects if they are not properly taken into account. In addition, significant values are still found on the truncated wing (the right in our example) of the interferogram (see Fig. 1), compounding the problem.

Therefore, it is necessary to extrapolate on both ends these interferograms as faithfully as possible. Since they will then be subject to Fourier Transformations, these extrapolations must preserve the initial spectrum as much as possible. Fortunately, it is possible to obtain

such properties by using autoregressive (AR) models [10,11]. Here we found that limited-order AR models (less than 10) were sufficient to capture the important properties of the interferograms. We introduce in Fig. 3 the interferogram obtained from the spectrum defined in Fig. 2 and we show how well its extrapolated parts fit with the original truncated part.

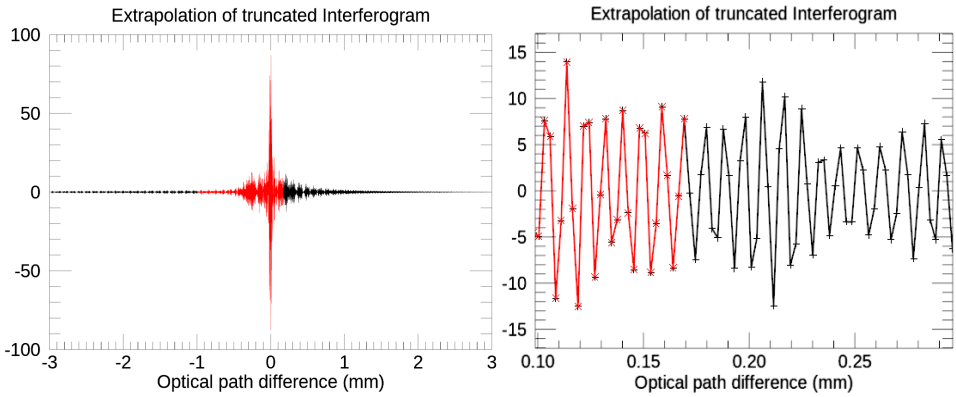

Fig. 3 : The original truncated interferogram from the spectrum of Fig. 2 is in red and the extrapolated signal is in black. On the left, we show the full extrapolated signal from a low order autoregressive model. This model is calculated only on the decreasing part of each side of the interferogram to better catch its decreasing property. On the right, we zoom in on the joining between signals to show its good fit to the original signal.

Fig. 4 shows that the modified signal keeps roughly the same spectrum as the original one.

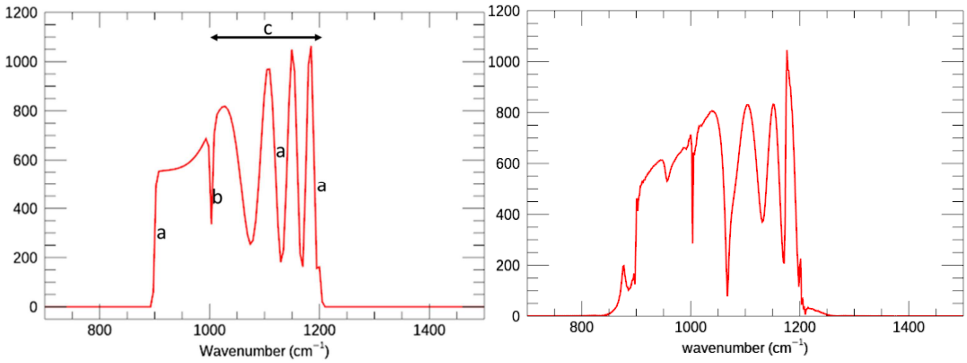

Fig. 4 : Left, the original spectrum is reproduced. Right, we show the spectrum calculated from the extrapolated signal of Fig. 3,. Note how well the bandpass nature of the original signal is respected as well as the largest oscillations.

All further processes to reconstruct the original, perfectly symmetric and regularly sampled interferogram will use this auto-regressive extrapolation.

3.2 Correcting the irregular sampling

We show here how to obtain a regularly sampled interferogram from its initial irregular sampling without damaging the underlying spectrum. First, in order to analyze the quality of the process of spectrum estimation from these imperfect interferograms, we need to insure the quality of our simulation.

While it is simple to generate an interferogram from knowledge of the spectrum, including its chromatic phase by a Fourier Transform, it is less straightforward to generate an interferogram sampled on an irregular grid by using the same tool (for consistency). In

particular to do this, we must first define a regular grid on which the interpolation will be performed to achieve the irregular values we need.

To avoid extrapolation, this regular grid will be defined by a ramp from the lowest to the highest OPD values over as many samples as in the irregular sampling of the initial OPD. The irregular OPD is then expressed in relation to this newly defined regular OPD sampling scale (see Fig. 5).

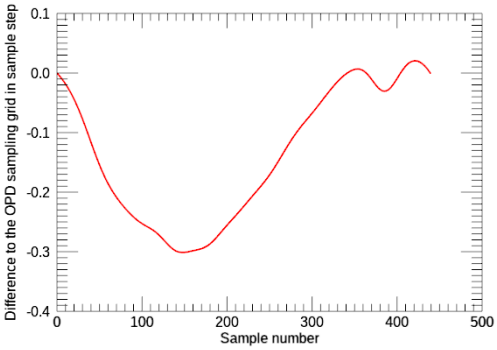

Fig. 5 : Deviation of the OPD from the regular OPD scale expressed in OPD sampling units. One unit being 2.7 µm. Values measured on the Sieleters LWIR instrument.

3.2.1 Interpolation step

Interferograms are band-limited because spectral filters installed in the instrument limit the spectrum of the incoming light. The Nyquist rule is then fulfilled, and therefore the Fourier shift theorem can be used to interpolate the interferograms at any sampling position without damaging the underlying signal.

Since the interferogram has been directly defined in Fourier space, it is already periodized and therefore no errors will be introduced by the shift theorem due to possible edge discontinuities.

As the shift theorem translates the whole grid by the same displacement value, this process must be repeated for each point in the interferogram (except for the first and last point of the interferogram, by construction). We give an example of the resulting interferogram in Fig. 6.

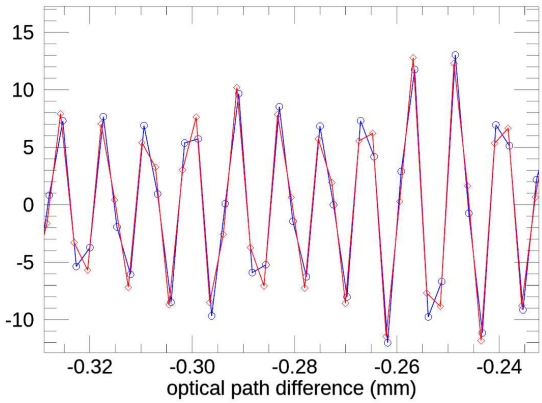

Fig. 6 : Comparison of the irregular and regular sampling of the interferogram ofFig. 3. The regular interferogram is in blue while the irregularly sampled interferogram is in red. Since they are plotted against their real OPD abscissa and the Nyquist condition is met, the two plots describe exactly the same signal.

However, since the evolution of the OPD is very smooth and limited in range, we need to demonstrate that such small deviations will nevertheless damage the resulting spectrum if they are not compensated or corrected. In the following step, we performed the Fourier transform of the irregularly sampled interferogram as if it was regularly sampled and supplemented by the correct values for the missing right wing and then phase-corrected by the exact phase. The resulting spectrum is given in Fig. 7.

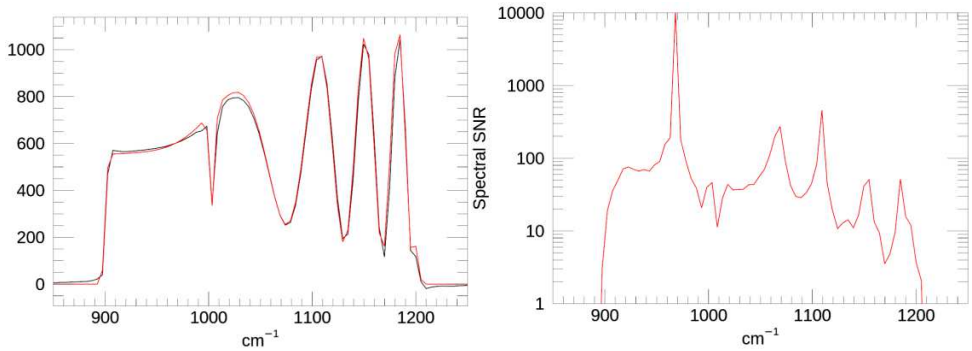

Fig. 7 : On the left we plot the true spectrum in red against the spectrum in black calculated from the irregularly sampled interferogram of Fig. 6. On the right, we give the spectral SNR of this spectrum estimator. The median SNR over relevant wavenumbers is 40.

Thus we have shown that even the modest departure from the OPD linearity on the FPA shown in Fig. 5 is enough to condemn the ambition of the instrument's spectral SNR (between 150 and 200, depending on the wavenumber [5]).

Therefore, we must correct these deviations to a regular sampling grid. Note that we have anticipated here the use of the spectrum estimation which will be explained later in this paper (cf. 3.3). It is indeed always preferable to evaluate a method on the relevant criterion, here the SNR of the spectrum.

3.2.2 Correcting irregular sampling

To improve our spectrum estimator we need to obtain a linear OPD sampling, thus we need an interpolation method on nonuniform samples whose spectral preservation properties are compatible with the desired spectral SNR. Among the available methods we chose to compare a simple Fourier based solution to a functionally weighted Lagrange interpolation [12] of greater sophistication and complexity.

Our Fourier solution takes advantage of the fact that, in this particular case, the sampling step is locally almost regular. Thus we simply applied the shift theorem used to create the irregular sampling of 3.2 but with –OPD instead of +OPD to reverse the displacement of the sampling grid and thus approaching the original regular sampling. The stronger the oversampling in Fourier space, the better.

Since this solution is built on the hypothesis that the initial sampling is regular, it can only be an approximation.

Thus we introduced the functionally weighted Lagrange interpolation which solves the oscillation problem between sampled points by weighting down the usual reconstructing Lagrangian basis functions and thus limiting oscillations (see Fig. 8).

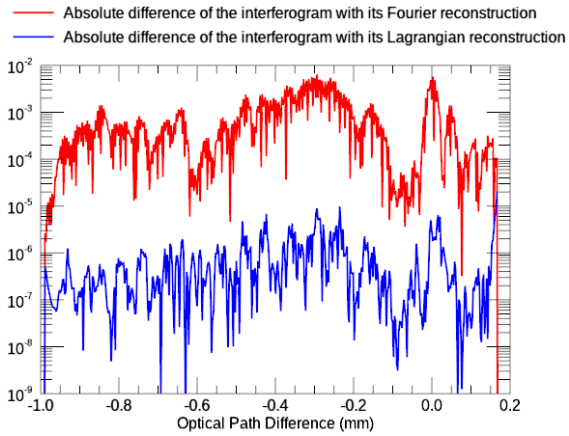

Fig. 8 : Comparison of errors made by Fourier and weighted Lagrangian reconstruction methods.

The precision of the functionnally weighted Lagrangian method [12] is regularly thousands of times higher than that of the Fourier transform. Thus with an SNR greater than one million, this processing step will not degrade the quality of the signal spectrum.

3.3 Spectrum calculation from an incomplete interferogram

We now focus on the spectrum estimation. The biggest challenge in this calculation is the quality of the phase estimation and its subsequent use.

There are many culprits that explain an erroneous phase (Fig. 2), some of them producing a non-linear phase [1]. Unfortunately, this means that the Zero Path Difference (ZPD) is undefined and thus there is an ambiguity in defining the center of the interferogram.

This is troublesome since the phase measurement should be done on the centered and balanced interferogram extracted from the asymmetrical initial interferogram (of Fig. 3). And we have, to our knowledge, no way to know it beforehand.

Thus we propose to test iteratively all likely centers until we find the best one. All that remains to be done is to define the criterion for doing so.

3.3.1 Centering the phase-distorted interferogram

We choose to use the quality of the final spectrum as a criterion, since it is the end result of the whole process. Because we won't know in advance the spectrum we will measure, it is impossible to use any error function, thus we simply tested the non-trivial property that spectra possess: their positivity. So we will simply choose the center that gives the least negative parts on the whole final spectrum. Fig. 9 gives an example of spectrum miscalculation.

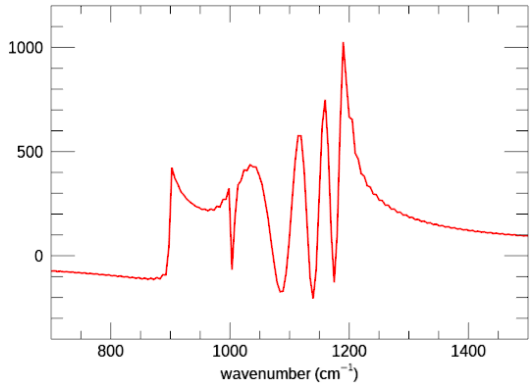

Fig. 9 : Spectrum obtained by our final estimator by shifting the center of the interferogram under test by 7 samples.

This procedure is surprisingly effective. We have simulated a very large phase dynamic, up to 60 radians with the same phase shape, without error. Thus, at the cost of an iterative procedure, we are able to find perfectly the center (see Fig. 10) of the underlying interferogram.

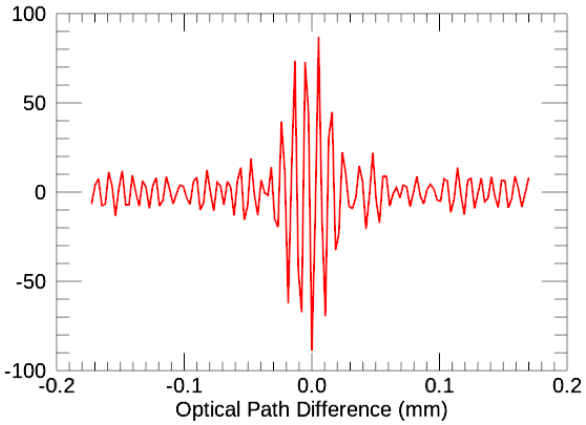

Fig. 10 : Symmetrical part of the interferogram of Fig. 3.

3.3.2 Producing a phase-correcting convolution kernel

The phase thus measured can be used to correct the spectrum in Fourier space (as in Mertz-like methods). However, the use of the Forman [6] method requires producing a convolution kernel in “real” space with good localization properties.

This kernel is classically obtained by taking the inverse Fourier Transform of the phase measured on the symmetrically part of the interferogram (see Fig. 10). Since we are only interested in a given spectral range and because out of band phase measures are unreliable, it makes sense to use only the phase defined on these frequencies (see Fig. 11).

But if we simply and classically zero this phase on out-of-band frequencies we produce a weakly decreasing convolution kernel (see Fig. 12).

Such wide and weakly decreasing kernel means that the convolution will use a lot of extrapolated points (up to a tenth of the interferogram) of dubious relevance to the true interferogram, thus damaging it. Worse, missing samples are often simply set to zero, which

unbalances the convolution. That's why in Forman's method, there is an additional phase apodization step which increases the rejection strength (see Eq. (2)).

$$A_{Forman}(\delta)=\left[1-\left(\frac{\delta}{\Delta}\right)^2\right]^2,\ \delta \text{ being the OPD and } \Delta \text{ is the OPD max value} \qquad (2)$$

The resulting kernel has a much better rejection and is decreasing faster than before (see Fig. 13).

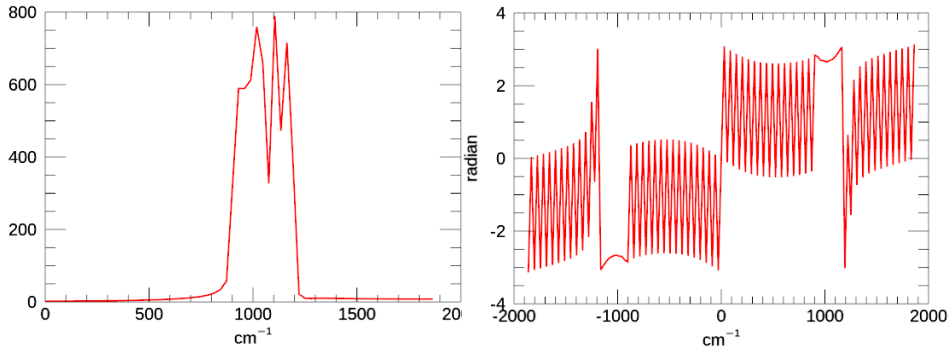

Fig. 11 : On the left, the absolute value of the spectrum obtained from the interferogram of Fig. 10, notice that it doesn't reach 0. On the right, the wrapped phase of the spectrum. Out of band values aren't well defined and thus are in practice random.

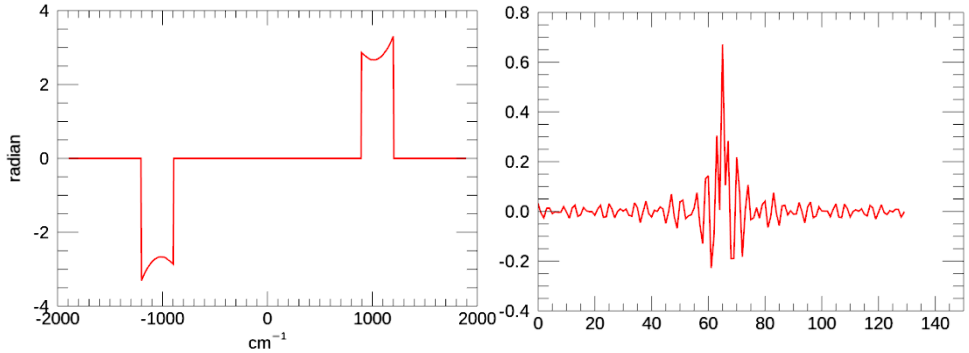

Fig. 12 : On the left, zeroing the phase of Fig. 11 at frequencies outside the spectral band of interest. On the right, the inverse Fourier Transform of the doctored phase on the left. Rejection at end-points is only a few tens.

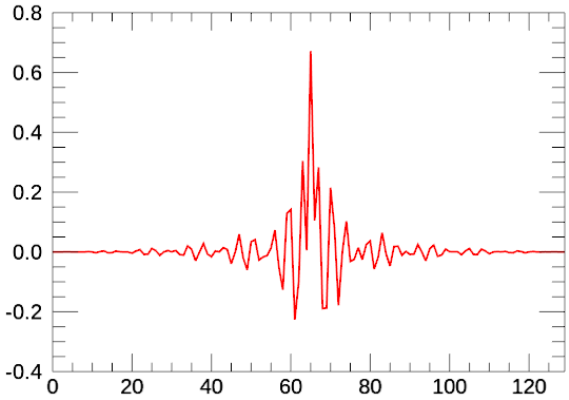

Fig. 13 : Convolution kernel obtained by multiplying the kernel of Fig. 12 by the Forman apodization function A_{Forman} of Eq. (2).

Unfortunately this step is potentially as damaging as the asymmetrical ponderation of the Mertz method. Let's write Mertz and Forman estimator in Eq. (3).

$$\begin{aligned} S_{Mertz}(\sigma) &= [I(\delta) \times \widehat{A_{Mertz}}(\delta)](\sigma) \times e^{-2i\pi\sigma\varphi(\sigma)} \\ &= \left[\left(S(\sigma) \times e^{2i\pi\varphi\theta(\sigma)}\right) * \widehat{A_{Mertz}}(\sigma)\right] \times e^{-2i\pi\sigma\varphi(\sigma)} \\ S_{Forman}(\sigma) &= \left[I(\delta) * \left(\left[e^{-\widehat{2i\pi\sigma\varphi(\sigma)}}\right] \times A_{Forman}(\delta)\right)\right] \\ &= S(\sigma) \times e^{2i\pi\sigma\varphi(\sigma)} \times \left[e^{-2i\pi\sigma\varphi(\sigma)} * \widehat{A_{Forman}}(\sigma)\right] \end{aligned} \quad (3)$$

I(δ) being the regularly sampled interferogram with phase φ(σ), S_{Mertz} and S_{Forman} being the Mertz and Forman spectrum estimator and φ (σ) being the wavenumber dependent erroneous phase of the interferogram. $A_{Mertz}(\delta)$ and $A_{Forman}(\delta)$ are the functions respectively used by Mertz and Forman to balance the OPD and apodize the convolution kernel (see Fig. 14).

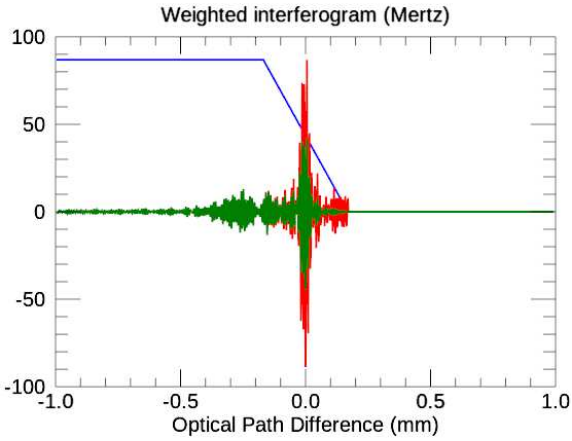

Fig. 14 : In red is the initial incomplete interferogram. In green is the multiplication of the truncated interferogram by the balancing function OPD before the Fourier Transformation and phase correction. In blue is the balancing function A_{Mertz} used to equilibrate the OPD.

These equations show that these induced perturbations of the spectrum cannot be easily compared since they occur at different stages.

But we can see in Fig. 15 how these functions distort the spectral shape we built in Fig. 2.

Although we did not incorporate the Mertz apodization on the left interferogram part because our extrapolation makes it unnecessary, we still find (see Fig. 15) that Forman's SNR is more often greater than Mertz's SNR [13].

But on the other hand it seems that Forman's method fails much more strongly than Mertz's when against the strongly rising curve found at the lower edge of the spectral band. Unfortunately since such situations are ubiquitous, it becomes difficult to choose one over the over.

Fortunately, improvement can be made without the need for additional and disruptive features. We just have to observe that the phase of Fig. 12 is, by design, made up of discontinuous signals. And discontinuous signals have their Fourier Transform well spread, which gives the low rejection kernel of Fig. 12.

The solution is simply to get rid of these discontinuities by joining the phase at its boundaries with straight lines (see Fig. 16). Such a manipulation is possible because no information is sought on frequencies affected by this new phase, so that no damage will be done to the spectrum concerned. It is even possible to go further by removing discontinuities on the derivative of the phase signal, to go from a C^0 solution to a C^n solution.

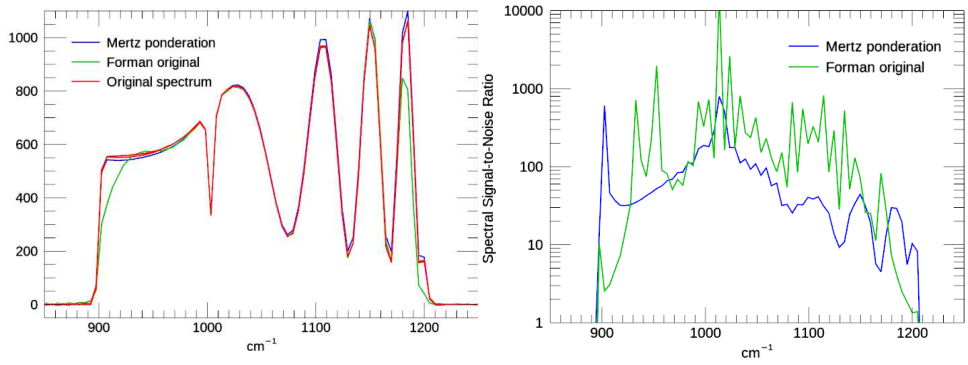

Fig. 15 : On the left, we plot the spectra in a linear scale: in red, the original spectrum, in blue, Mertz's estimate and in green, Forman's estimate. The original spectrum is made to cover other curves, so when green or blue are apparent, it means that there are noticeable errors. On the right, we give the spectral signal-to-noise ratio of each estimator.

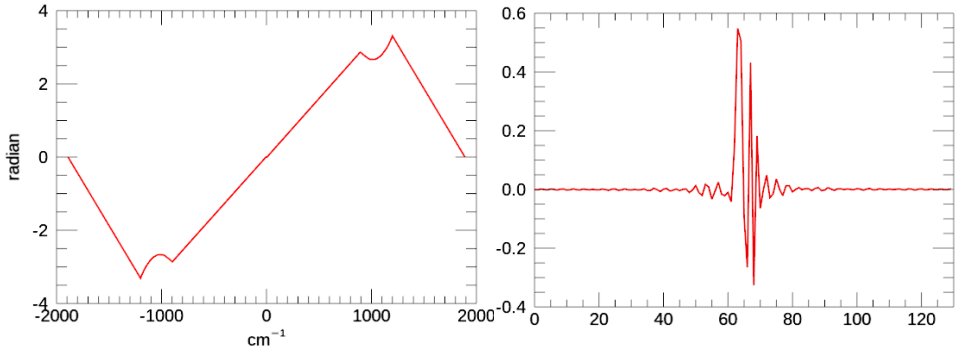

Fig. 16 : On the left, the synthetic phase realized by connecting the useful spectral values of Fig. 12 by straight lines. On the right, is the convolution kernel obtained by inverse Fourier Transform of the synthetic phase on the left. Rejection at end-points is better than 500.

This simple operation already considerably improves the quality of spectrum estimation in Forman's method, but it can even be improved by increasing the spectral resolution of the phase up to the final sampling grid. This is simply done by classical linear interpolating

method in Fig. 16, thus encoding implicitly more information on the smoothness of the phase. All subsequent spectrum estimators will use this interpolated phase.

But the use of this kernel, however "sharp" it may be, requires an extrapolation of the interferogram since its end-points do not have half of the data needed to compute the convolution. It seems to us that this signal processing step is most often ignored in theoretical development and left to undocumented procedures.

Unfortunately, this missing data, no matter what we do, will be defined. Their definition is explicit when using the Forman [6] convolution method but implicit when using the Mertz [7] method because it operates in Fourier space. In the latter case, the missing data is silently replaced by the data at the other end of the interferogram because of enforced interferogram periodization.

But it is indeed reasonable to expect that by using a more reliable interferogram extrapolation the quality of the phase correction will increase. We will therefore use the solution in paragraph 3.1 which increases the interferogram size by extrapolation to exploit all the values of the convolution kernel (Fig. 12&Fig. 16). The aberrant phase will then be corrected either in Fourier space either in real space.

Then, it is important that the wing of the untruncated interferogram is simply duplicated on the other wing since the phase-corrected interferogram should be now symmetric but is not in practice because of the extrapolated data added on the shortest wing.

In Fig. 17, we compare these two new estimators, which are devoid of any filtering steps, with the legacy estimators.

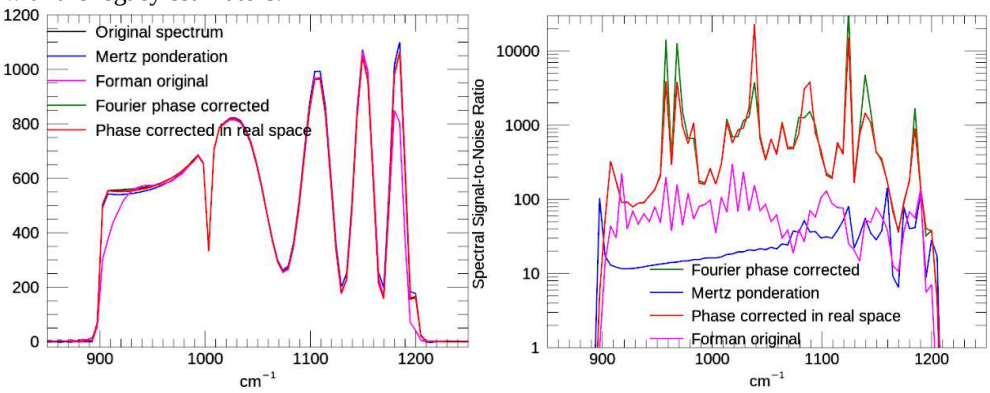

Fig. 17 : On the left, we have represented all spectral estimators with respect to the original spectrum. On the right, we give the spectral signal-to-noise ratio of each estimator.

Unfiltered estimators are much better than the estimators inherited from Mertz and Forman, thanks to the abandonment of apodizations that prove to be harmful. It can also be noted that real space or Fourier space estimators are almost perfectly equivalent, which is theoretically expected.

4. Conclusions

The advent in the real world of static Fourier Transform Spectrometers which have a very limited optical path difference range, gives greater practical importance than before to the process of extracting the spectrum from truncated histograms. As these instruments rely heavily on signal processing, we have chosen to study only this part by performing numerical experiments.

After demonstrating the quality of the numerical simulation of realistic defects affecting these instruments, we proved that predictable experimental defects such as irregular OPD sampling and non-linear phase can, and should, be compensated for. At the same time, we

showed that the classical methods of Mertz and Forman caused large spectral errors. However, the classical solution of smoothing discontinuities in signals that will need to be transformed by a Discrete Fourier Transform, in the real or spectral domain, has proved sufficient to lead to new, well behaved spectrum estimators.

Finally, it should be noted that the performance of these estimators is strongly dependent on the shape of the spectrum being measured.

Further studies will involve the analysis of the amount of interferogram symmetry needed to reliably evaluate the non-linear phase and its impact on performance. Future work will move backward in the acquisition pipeline and will explore the impact of image resampling on the spectra.

Funding

ONERA

Acknowledgements

We would like to thanks the entire Sieleters team responsible for the design, building and operation of this instrument and who made it available for other uses. We also want to thank the Direction Générale de l'Armement (the French Ministry of Defense) for its funding of the instrument and interest in this work.

We also would like to thank the anonymous reviewers who helped us make this paper much better.

Disclosures

The authors declare no conflicts of interest.

5. References

1 P. R. Griffiths and J. A. De Haseth. *Fourier transform infrared spectrometry*. Vol. 171. (John Wiley & Sons, 2007).

2 G. Stroke and A. Funkhouser. "Fourier-transform spectroscopy using holographic imaging without computing and with stationary interferometers.", Phys. Let. 16, 272 (1965).

3 E. Puckrin, C. S. Turcotte, P. Lahaie, D. Dubé, P. Lagueux, V. Farley, F. Marcotte and M. Chamberland, "Airborne measurements in the infrared using FTIR-based imaging hyperspectral sensors," Electro-Optical Remote Sensing, Photonic Technologies, and Applications III, 7482. International Society for Optics and Photonics, (2009).

4 A. Lacan, F-M. Bréon, A. Rosak, F. Brachet, L. Roucayrol, P. Etcheto, C. Casteras and Y. Salaün, "A static Fourier transform spectrometer for atmospheric sounding: concept and experimental implementation," Optics express **18**.8 (2010).

5 C. Coudrain, S. Bernhardt, M. Caes, R. Domel, Y. Ferrec, R. Gouyon, D. Henry, M. Jacquart, A. Kattnig, Philippe Perrault, L.Poutier, L. Rousset-Rouvière, M. Tauvy, S. Thétas and J. Primot "SIELETERS, an airborne infrared dual-band spectro-imaging system for measurement of scene spectral signatures." Optics express **23**.12 (2015).

6 M. L. Forman, W. H Steel and G. A Vanasse, "Correction of asymmetric interferograms obtained in Fourier spectroscopy." JOSA **56**.1 (1966).

7 L. Mertz. "Auxiliary computation for Fourier spectrometry." Infrared Physics **7**.1 (1967).

8 A. Kattnig, "Theoretical and practical analysis of spatial and spectral calibration of static Fourier transform infrared spectrometers." Optics express **27**.10 (2019).

9 M-L. Junttila, J. Kauppinen, and E. Ikonen, "Performance limits of stationary Fourier spectrometers." JOSA A **8.9**, (1991).

10 X. Liu, S. Chen, D. Cui, X. Yu and L. Liu, "Spectral estimation optical coherence tomography for axial super-resolution." Optics express **23**.20 (2015).

1. 11 J. Durbin, “The fitting of time-series models.” Revue de l’Institut International de Statistique, 1960.

12 J. Selva, "Functionally weighted Lagrange interpolation of band-limited signals from nonuniform samples." IEEE Transactions on Signal Processing **57**.1 (2008)

13 L. D. Spencer. “Imaging Fourier transform spectroscopy from a space based platform: the Herschel/SPIRE Fourier transform spectrometer”. Diss. Lethbridge, Alta.: University of Lethbridge, Dept. of Physics and Astronomy, 2009.